DESIGN OF PLANAR REFLECTOR ANTENNAS

Stanislav GOŇA, Zbyněk RAIDA
Dept. of Radio Electronics
Brno University of Technology
Purkyňova 118, 612 00 Brno
Czech Republic

Abstract

A design of single and folded reflector antennas is presented. We focus in the use of an optimization during the design process. In comparison to existing papers, possibility of realization of folded antenna at X band frequencies is demonstrated. Further more, an original procedure of phase center extraction of antennas and scatters is described. The procedure is applied in the design of simple reflector antenna incorporating a non-hyperbolic, electrically small reflector.

Keywords

Reflector antenna, geometrical optics, constrained optimization, Huygen's principle

1. Introduction

Planar reflector antennas attracted enormous attention of many designers during last decade. The antennas exhibit comparable efficiency as the standard curved reflector antennas but have the advantage of ease of manufacture at low cost. Basically, two groups of the antennas exist. First one could replace the standard parabolic dish, and in this paper, we refer it as a simple reflector antenna [1]. The second one could be viewed as a novel type of Cassegrain antenna. The antenna became known as folded reflector antenna [2]. In this case, the blockage effect known by designers of Cassegrain systems is neglected. Thus, good aperture efficiency of the overall antenna might be achieved. If carefully designed, aperture efficiency might be as high as 70%.

The high sensitivity of phase of reflection coefficient from patches on tolerances in manufacture process is the common disadvantage of planar reflector antennas [1]. Typically, change of the patch dimension by $\lambda_0/30$ corresponds to the phase change of 100°. The maximum phase error of ~ 20° (of a single patch shifter) for the antenna operating at X band is guaranteed if the maximal etching error is around 250 μm. For the antenna operating at W band, patch dimensions must be within 25 μm tolerance. An achievement of such accuracy might be a real problem for substrates with metallization thickness of 17 μm or 35 μm when tasking the job to the standard PCB makers. As a result of dimension tolerances, radiation parameters of the antenna are then corrupted.

In order to decrease sensitivity of reflection coefficient on patch dimensions, multi-layer flat reflectors have to be incorporated. As shown in [3], much less sensitivity could be obtained.

This article is focused in the design of planar reflector antennas with main reflector consisting of a single layer of patches placed on a substrate and optionally covered by superstrate (ensures protection against aggressive environment, gold plating of the patches is then not necessary). Incorporation of the superstrate causes a small shift of the resonance (occurs for lower patch dimensions) but doesn't influence the tuning range and sensitivity of the phase of reflection coefficient on patch dimensions.

Following sections will describe design strategy using local optimization techniques based on LV (Levenberg-Marquardt) method [4]. Several examples are given in order to demonstrate functionality and efficiency of the design. Operating frequency was chosen to be in middle of X band for all given examples. Thus, existing commercial full wave programs based on method of moments might be used to verify antennas designed by Matlab program.

Besides of radiation properties, feed related problems are discussed.

2. Planar Antennas - Arrangement

In similar to [1], [2], the design of simple or folded reflector antenna has been carried out. An arrangement of these antennas is shown in Fig. 1. Both antennas are of substrate of thickness d_1 with metal patches on a top of the layer. Optionally dielectric cover may be included. Incorporation of the effect of dielectric cover is based on originally extended theory of [5]. The complete equations were published in [6]. Several representative rays are shown in Fig. 1. Their traces are easily to found by laws of geometrical optics.

Separation between reflectors is denoted as L while D is the main reflector diameter. Both antennas are typically fed by a horn antenna with an appropriate surface of the aperture in order to illuminate slot array or hyperbolic reflector. A small microstrip array is another alternative of feeding we use in this article. A small impedance bandwidth is disadvantage of the array feed, further reduction of profile of the antenna is advantageous.

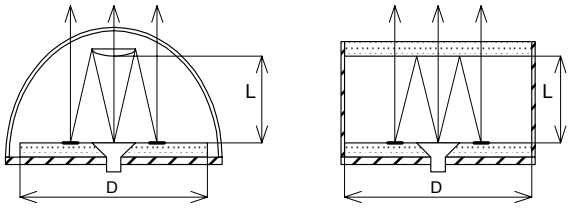

Fig. 1 Simple reflector antenna with a radome (on the left) and folded reflector antenna (on the right)

2.1 Design Strategy

When designing a planar reflector antenna, one has to go through all cells of the main reflector and adjust patch dimensions to get in-phase reflected field in the plane of the main reflector. The delay of non-center traveling rays can be easily evaluated by goniometric relations.

Regardless of the type of the antenna, orientation of tangential component of incident electric intensity in the middle of a particular patch is always the same. The orientation is shown in Fig. 2.

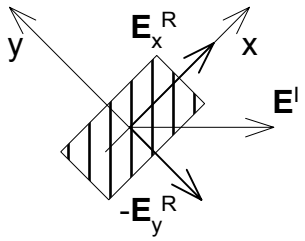

Fig. 2 Orientation of the vector of electric field intensity E^I of incident wave (tangential components) and components E^R_x, E^R_y of reflected wave.

Components of intensity of the reflected wave (denoted as E_x^R or $-E_y^R$) inhibit a phase behavior shown in Fig. 3 (at normal incidence). In case of non-normal incidence, similar charts could be obtained. The only difference is that the larger angle of incidence leads to larger resonance dimensions. This fact has to be kept in mind choosing cell[1] dimensions large enough (typically 0.8 λ_d, resp. 0.55 λ_0).

In case of a simple reflector antenna, components E_x^R and $-E_y^R$ have to be in phase, while for the folded reflector antenna, 180° phase shift between the two components has to be achieved.

Dependencies shown in Fig. 3 were computed using the spectral domain method. Current density on the patch was modeled by large domain basis functions [5]. Only two Floquet modes ($P = Q = 2$) and 121 space harmonics were used ($M = N = 5$).

To find out dimensions of patches, an optimization technique had to be used. The next section describes LV method [4], which is very efficient and robust for that task.

[1] The area of the main reflector is divided into rectangular or square regions called cells.

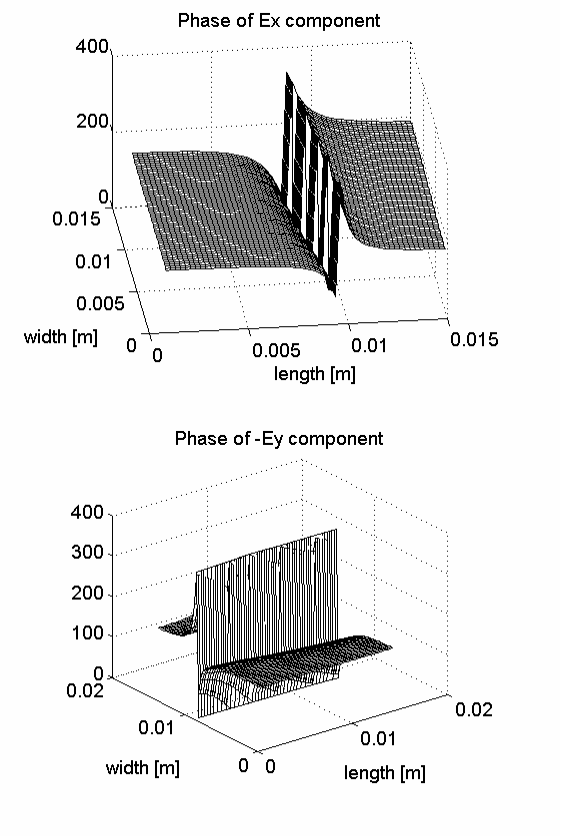

Fig. 3 Phase of components E_x^R and $-E_y^R$ of wave reflected from central patch of the main reflector. We assume normal incidence ($\vartheta^I = 0°$, $\varphi^I = -45°$), cell dimensions $a = b = 16$ mm, substrate permittivity $\varepsilon_r = 2.22$ and thickness $d = 1.5$ mm.

2.2 Levenberg- Marquardt Method

The method [4] was further extended to allow constraint optimization[2] and offer better step length control.

Optimization problem to be solved by LV method can be described as follows

$$|| \mathbf{F}(\mathbf{c}) - \mathbf{F}_d ||= 0 \quad ; \ \mathbf{c} = \mathbf{c}_{min} - \mathbf{c}_{max} \tag{1}$$

where **F** is a vector non-linear function. Each component of the function may depend on several design variables (DV), which are stored in vector $\mathbf{c}_i$ (state vector at i^{th} iteration). $\mathbf{F}_d$ represents the vector of desired function values. In case of planar reflector antenna, the function **F** and state vector $\mathbf{c}_i$ is of the form

[2] The original application in [4] used the unconstrained version of Levenberg-Marquardt method only. Addition of constraints on design variables is simply done by saturating values of those design variables, which tend to go out of bounds. Remaining design variables, which are still within allowed bounds, may further change. Stepping on boundary is thus ensured.

$$\mathbf{F} = \begin{bmatrix} \arg(E_x^R(x,y)) \\ \arg(-E_y^R(x,y)) \end{bmatrix}, \quad \mathbf{c}_i = \begin{bmatrix} a' \\ b' \end{bmatrix}.$$

LV algorithm iteratively performs steps of state vector $\mathbf{c}_i$. These steps are based upon evaluation of Jacobian of the function **F**. After several steps, algorithm delivers a result, which is optimal in least-square sense. Subsequent paragraphs give a commented list of steps iteratively performed by LV method.

1. First, the difference between the initial (or actual) value of **F** and the desired one $\mathbf{F}_d$ is evaluated

$$\Delta\mathbf{F} = \mathbf{F}_i - \mathbf{F}_d . \tag{2}$$

2. Second, Jacobian at $\mathbf{c}_i$ is numerically evaluated and stored in the matrix [D]. Since Jacobian is known, the step length $\Delta\mathbf{c}_i$ can be expressed in the from

$$([\mathrm{D}]^H[\mathrm{D}] + \alpha[\mathrm{I}])\Delta\mathbf{c}_i = [\mathrm{D}]^H \Delta\mathbf{F} \tag{3}$$

where α is a regularization parameter.

Expressing $\Delta\mathbf{c}_i$, either direct inversion (resp. Gaussian elimination) or singular value decomposition (SVD) can be used. SVD is advantageous for ill-conditioned problems. The choice of the regularization parameter is done using the empirical equation [4]

$$\alpha = \frac{\beta\ \mathrm{Trace}([\mathrm{D}]^H[\mathrm{D}])\,\|\,\mathbf{F}(\mathbf{c}_i) - \mathbf{F}_d\,\|^p}{N\,\|\,\mathbf{F}_d\,\|^p} \tag{4}$$

where N stands for the number of DV's and p is of the meaning of exponent (it typically equals to 2).

Other alternatives of getting α (generalized cross validation method) exist [4]. They were not tried out.

3. Third, the function is evaluated in a new point $\mathbf{F}_c+\Delta\mathbf{c}_\alpha$. Then, the difference between the current and desired function is evaluated. Depending on the value of the difference for the current point and the previous one, following cases may appear:

- the error has increased (step length is reduced to one half of the current value);
- the error has become smaller (no action);
- the error has decreased only slightly (step length is doubled).

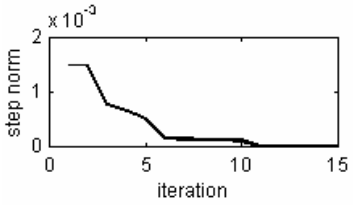

Fig. 4 Evolution of the length of step during dimension tuning. Curve corresponds to the central patch of folded 225 mm reflector antenna (see examples below). The curve shown is atypical since the patch is at resonance. In the case of non-resonating patch, only 5 to 6 iterations are necessary.

The algorithm then iteratively performs the above-described steps until specified criteria are reached (the error norm dropped below the required value or the number of iterations exceeded the specified value).

An example of one optimization run of LV method is shown in Fig. 4. We can see that after a few steps, the step becomes very fine, which corresponds to the decrease of the error norm below the specified value (the norm of phase errors <2°).

3. Far-Field Patterns

Once patch dimensions of the array are known, far-field radiation pattern might be obtained by summing reflected field from all cells. Mathematically written:

$$\begin{bmatrix} E_\vartheta \\ E_\varphi \end{bmatrix} = \sum_{i=1}^{Nc} -\frac{\mathrm{j}k}{4\pi} \begin{bmatrix} Q_{11} & Q_{12} \\ Q_{21} & Q_{22} \end{bmatrix} A \frac{\mathrm{e}^{-jk\Delta r_i}}{r_i} \tag{5}$$

- matrix Q can be expressed as

$$\begin{bmatrix} Q_{11} & Q_{12} \\ Q_{21} & Q_{22} \end{bmatrix} = \begin{bmatrix} Z_0\mathbf{J}\cdot\mathbf{T}_{xyz\_\vartheta} & \mathbf{K}\cdot\mathbf{T}_{xyz\_\varphi} \\ Z_0\mathbf{J}\cdot\mathbf{T}_{xyz\_\varphi} & -\mathbf{K}\cdot\mathbf{T}_{xyz\_\vartheta} \end{bmatrix}$$

  J and **K** stand for equivalent electric and magnetic current densities. These are determined from Floquet mode (0,0) amplitudes of electric or magnetic intensity of reflected wave.

- **T** vectors perform Cartesian to spherical transformation of field quantities.

- Constant A is obtained by integrating field distribution of Floquet (0,0) mode across the surface of a particular cell. Resulting value of such integration across cell dimensioned a and b is

$$A = a\,b\ \mathrm{sinc}\left[k_x a/2\right]\mathrm{sinc}\left[k_y b/2\right] .$$

  Symbols k_x and k_y stack information about incidence and observation angles.

$$k_x = -k\sin(\vartheta^I)\cos(\varphi^I) + k\sin(\vartheta)\cos(\varphi)$$
$$k_y = -k\sin(\vartheta^I)\cos(\varphi^I) + k\sin(\vartheta)\cos(\varphi)$$

- Symbol Δr_i stands for space delay of ray which points out of the particular cell center at $[\vartheta, \varphi]$ direction with respect to the central ray, k is free-space wave number.

4. Examples

4.1 Folded Reflector Antenna

The following table gives physical dimensions and antenna parameters for a version of the folded reflector antenna. Antenna was designed by means of Matlab pro-

gram Rarray. The total design time was about 20 minutes[3]. During the design, no assumption on symmetry of the layout of the main reflector was given, thus totally 129 patches had to be tuned. Average time for adjustment of dimensions of one patch was roughly 10 seconds. After successful design, postprocessor was initiated. About 5 minutes were taken to compute complete 3D radiation pattern of the antenna. Careful review of dimensions of patches of the main reflector of planar antenna showed that antenna inhibits half symmetry. Bottom part of the layout could be obtained by rotating the upper one by 180°.

Antenna diameter D [mm]	225 (7.5 λ_0)
Reflector separation L [mm]	37.5 (1.25 λ_0)
L/D ratio	1/6
Feeder	2 × 2 patch array
Main reflector	d_1 =1.5 mm, ε_{r1} = 2.22, tan δ_1 = 0.001, t_1 = 35 μm
Auxiliary reflector (slot array)	d_2 =1.5 mm, ε_{r2} =3.7, tan δ_2 = 0.005, t_2 = 35 μm

Tab. 1 Physical dimensions of the designed folded reflector antenna (operating frequency f = 10 GHz).

In order to verify radiation properties of the designed antenna, the commercial program IE3D (version 8) was used. Mesh density was set to be 10 divisions at highest frequency (11 GHz). Resulting number of equations was about 8000 and solution at one frequency took about 3 hours[4]. Feeding of the structure was done by 2×2 microstrip array via 4 localized sources. Antenna directivity at 10 GHz was determined from 3 dB beam-widths as

$$D = 27000/\left(2\Theta_E 2\Theta_H\right) = 27000/\left(9.6 \cdot 8.8\right) \Rightarrow 25.1\text{dB}.$$

The value is in a very good agreement with the value obtained from IE3D (24.8 dB).

Simulated directivity and side lobe vs. frequency are shown in Fig. 6. Given data cover frequency range from 9.25 to 11 GHz. At frequencies 9.75 and 10.25 GHz, IE3D returned magnitude of reflection coefficient higher than one due to a very rough mesh density. Drop in directivity is not present in reality at these frequencies. Finer meshing than 10 cells per wavelength would probably give realistic values. However, mesh refinement was not possible due to the limited computer memory. Iterative AIMS solvers were not successful at reaching the convergence. Other solvers were not tried out.

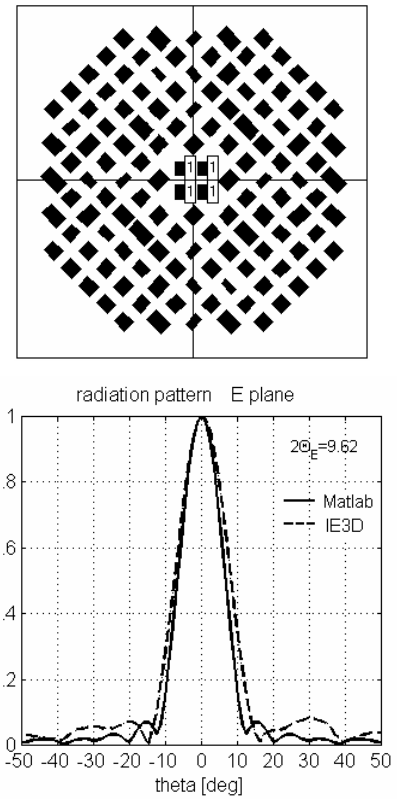

Fig. 5 a) Layout of the main reflector of the folded reflector antenna (f = 10 GHz, D = 225 mm, L = 37.5 mm). Slot array had a cell period of 12x6mm with 11x1mm slots.
b) Computed radiation pattern (Matlab vs. IE3D).

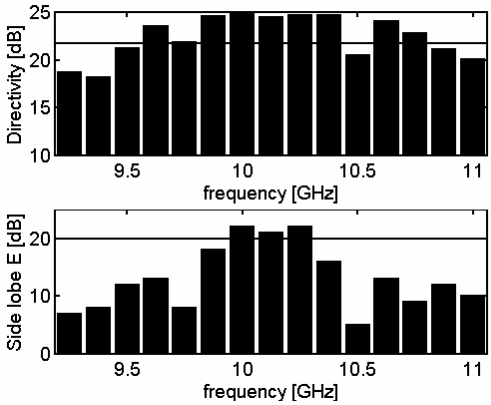

Fig. 6 Simulated (IE3D) directivity and side lobe level versus frequency (10 divisions per wavelength).

	Matlab	IE3D
Directivity [dB]	25.0	24.8
E-plane Beamwidth	9.62	11.13
H-plane Beamwidth	8.84	10.19
Gain [dB]	-	23.2
Radiation efficiency	-	73 %
Aperture efficiency		38 %

Tab. 2 Radiation parameters of the designed folded reflector antenna (f = 10 GHz, D = 225 mm, L/D = 1/6)

[3] Celeron 433 MHz, Windows 98 SE

[4] AMD Atholon 1.2 GHz, 768 MB RAM, AdvSym matrix solver, Windows 2000

4.2 Feeding of the Planar Antennas

4.2.1 Folded Reflector Antenna

When designing folded reflector antenna, the position of the phase center of the antenna feeder has to be known. Unfortunately, the position is not constant but it changes with respect to the observation distance. The antenna designer should ensure that the position of the phase center of the feeder is approximately in the level of the ground plane (for example $\pm\ \lambda_0/10$) of the main reflector (this condition is fulfilled for a sufficiently large distance L)[5].

Visual illustration of the phase center position for different feeders and constant observation distance L is shown in Fig. 7. The figure shows that waves in close proximity of the microstrip antenna are almost plane-like, while horn antenna produces spherical-like waves. As a consequence of that, the position of the phase center of the horn approximately coincidences with the ground for the given observation distance L (in our case 1.25 λ_0). Settling the position of the phase center of the microstrip antenna occurs at much larger distance (see Fig. 10).

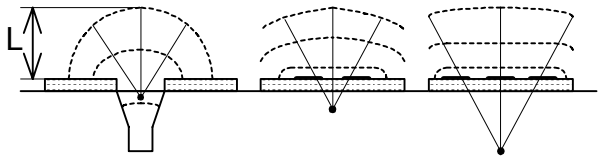

Fig. 7 Snapshots of several wavefronts of field radiated by a horn antenna (on the left), 2×2 and 3×3 element patch arrays (on the right). Dots show phase center position, which is valid for observation distance L.

At this point, we can pre-calculate the position of the phase center of the microstrip feeder in advance and use it during the design of the folded reflector antenna. Next paragraphs describe in detail the procedure of phase center extraction for a small patch array.

Let us assume an arrangement according to Fig. 8. Position of the actual phase center for a given patch array (in general any feeder or sub-reflector) may be determined from a snapshot of the electric field generated at some time point. Location of the phase center can be determined from

$$z_c = \frac{y_1^2 - (\lambda_0/2)^2}{\lambda_0} - z_1 \tag{6}$$

where λ_0 is free-space wavelength.

[5] Ideally, the phase center coincidences with the ground at infinity. In reality, observation of the phase center for a small horn antenna (aperture sized about $\lambda_0 \times \lambda_0$) at the distance of 1 to 2 wavelengths ensures the position of the phase center to be within the interval <0; $\lambda_0/10$>. On the contrary, small microstrip antenna (4 elements) has that distance about 5 λ_0 or more.

Let us emphasize that a more accurate extraction of the phase center position is done if the actual wavelength is substituted instead of λ_0.

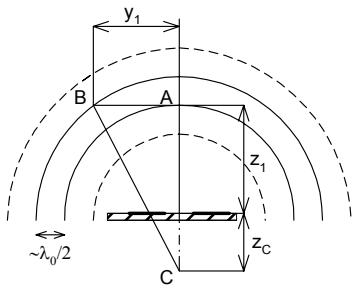

Fig. 8 Several wavefronts of field radiated by 2×2 patch array (extraction of the phase center of the antenna). Substrate is assumed to be infinite in extent.

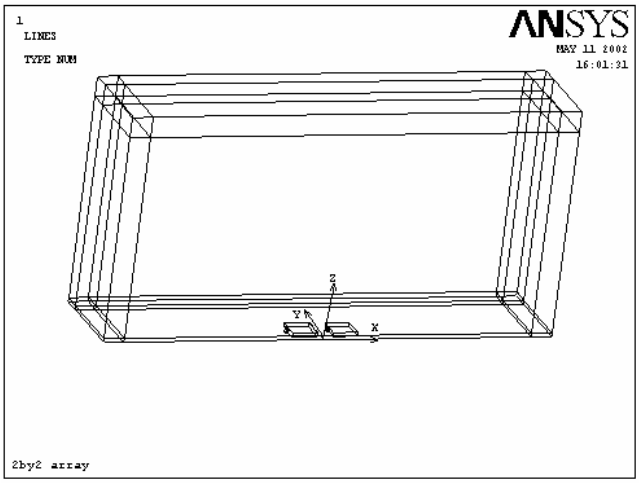

Fig. 9 Wire frame model of 2×2 microstrip array in ANSYS. Model used about 160.000 first-order tetrahedral elements. Global element size was set to 0.003 m. Patches were fed by in-phase current sources. Solution time was about 2 hours on 1.2 GHz Athlon computer (sparse matrix solver).

To be more specific, an example of the phase center extraction for 2×2 patch array, which is used as a feeder, is given. The antenna is located on an infinite dielectric substrate having permittivity 2.22 and thickness 1.5 mm. Due to the symmetry of the array, only half of the array was modeled. FEM model of the antenna is shown in Fig. 9 Computational domain was dimensioned to 150 mm × 86.5 millimeters × 30 mm. Thickness of the perfectly matched layer (PML) was $\lambda_0/4$.

After the solution of FEM problem, phase center extraction was done. The procedure was the same as in Fig. 8. Resulting dependence of the position of the phase center on observation distance is shown in Fig. 10. As mentioned above, the phase center position can be determined approximately and accurately. Thus two curves are shown. Phase center position corresponding to the reflector to reflector separation of L = 37.5 mm is then about 17 mm.

In order to validate that value, a folded reflector antenna was designed to respect the new position of the phase center. Comparison of the modified design and the original one (chapter 4.1) showed a slight decrease of directivity at the frequency 10 GHz (about 0.5 dB).

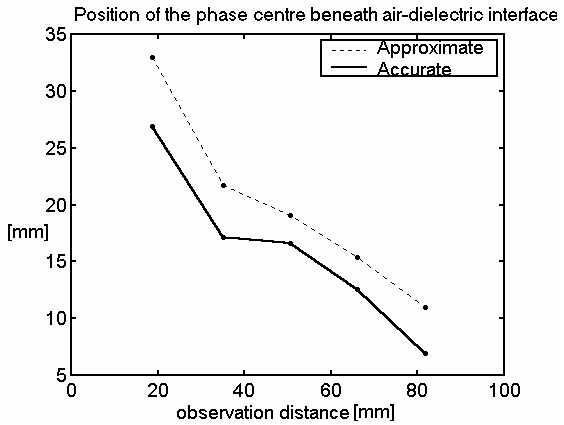

Fig. 10 Dependence of the phase center on actual observation distance for 2×2 patch array.

In spite of this fact the slot array seems to force position of the phase center to be at the origin. Thus, modification of the design for the folded reflector antenna is not necessary.

In order to examine behavior of 2×2 microstrip array as a feeder, the folded reflector antenna with the reflector-to-reflector separation L = 75 mm was designed. Similarly as in the previous case, the design respecting and not-respecting the phase center of the feeder was performed. Resulting directivity at the frequency 10 GHz dropped to 23.7 dB (no offset of the phase center considered) or 23.4 dB respectively (offset included).

On the basis of these experiments, we can conclude that the idea of the altered phase center position is not applicable in the case of the design of the folded reflector antenna. The phase center position certainly plays a role in the folded antenna. This was tested on the design having L = 75 mm, where 2×2 array was replaced by 3×3 one. As expected, the effective non-ground position of the phase center resulted in further drop of directivity to 19.4 dB (considering phase center on the ground).

We can conclude that the design of a folded reflector antenna being fed by a small array and having reflector and slot array in close proximity (about one wavelength) brings surprisingly good results, which might be of practical importance.

The next chapter explains the design of a simple reflector antenna where an idea of phase center extraction is applicable.

4.2.2 Simple Reflector Antenna

Usually, a hyperbolic sub-reflector is used if a simple reflector antenna is being designed. Incorporation of that reflector at X band antenna, which is of the diameter about 200 mm (~ 7 λ_0), restricts the diameter of the sub-reflector to roughly about 2 λ_0 (in order to have a small blockage effect and approximately plane wave illumination of the reflector). In this case, a standard hyperbolic reflector doesn't behave according laws of geometrical optics and its phase center has to be found out by employing the advertised technique. It is also advantageous to replace the hyperbolic reflector by non-hyperbolic one, which is easier to fabricate. The shape of the non-hyperbolic sub-reflector, which was chosen as a test case, is shown in Fig. 11. Reflector is of rotational symmetry. Numerical extraction of its phase center is done similarly as in previous sub-chapter. Its solid model in ANSYS is shown in the same figure.

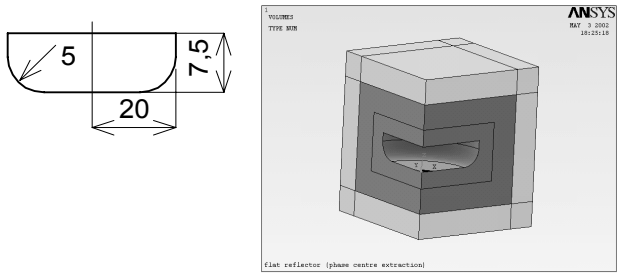

Fig. 11 Complete FEM model of the non-hyperbolic reflector (ANSYS 5.7), computational and PML volumes are shown in dark and light gray respectively. Auxiliary volume housing reflector served for definition of Maxwell surface flag (field transformation to any point out of the MXW surface via HFNEAR command). Model used first order tetrahedral elements with global element setting ESIZE,0.0015. Total number of elements and unknowns was 175.023 and 197.719 respectively. Solution took about 80 minutes on 1.2 GHz Athlon having 768 MB RAM installed.

Extracted dependence of the phase center position on the observation distance z, which is measured from the bottom of the reflector, is shown in Fig. 12.

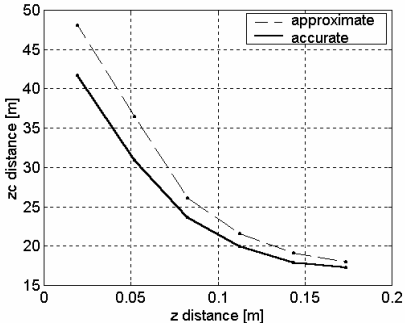

Fig. 12 Dependence of the phase center on the actual observation distance z for the non-hyperbolic reflector.

In order to verify the dependence of the position of the phase center on the observation distance, the design of a simple reflector antenna was done. We assumed that the phase center of the reflector is located 89 mm above the air-dielectric interface of the main reflector (see Fig. 13 for the complete antenna assembly). In order to set appropriate height of the slot array above the main reflector, Fig. 12 was used. Physical distance z_c has been found in such way to achieve the sum of the physical distance and distance z_c

equal to 89 mm. That condition was satisfied for separation L = 59 mm. Finally, full-wave simulation of the antenna for the separation interval L was performed (Tab. 3).

L [mm]	46	52	58	63	64	70
D [dB]	20.3	17.9	13.6	21.2	20.8	16.7
SL_E [dB]	12	10	4	15	15	7
SL_H [dB]	14	14	5	16	17	11

Tab. 3 Directivity and side-lobe level for the designed simple reflector antenna as a function of distance above the main reflector

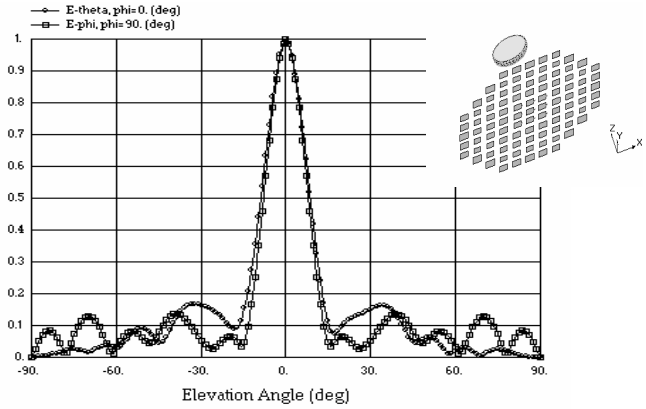

Fig. 13 Assembly of the simple reflector antenna and simulated radiated patterns for separation between reflectors L = 63 mm (E_υ (φ = 0) corresponds to E plane), D = 200 mm, f = 10 GHz.

As documented in Tab.3, maximum of the directivity corresponds to the value of L = 63 mm and not to L = 59 mm. In spite of this fact, the phase center position is not extracted at a very high accuracy. However in reality, the vertical adjustment of the sub-reflector is always present and the maximal directivity may be adjusted. As a feeder of the simple reflector antenna, 3×3 microstrip array of patches was used. Simulated radiation patterns (IE3D) are shown in Fig. 13.

5. Conclusions

A design of a simple reflector antenna and a folded one was presented. Although the results are not supported experimentally, full wave verification by a commercial software proved credibility of the obtained results.

The given example of the folded reflector antenna shows the possibility of realizing such an antenna at frequencies as low as 10 GHz. The resultant radiation efficiency and side-lobe of the antenna are very good. Metallic sidewalls of the antenna were not present in the simulation. This simplification was enabled due to the negligible level of the incident field on the edges of the main reflector. The design of the folded reflector antenna relied on the assumption that the phase center of the microstrip feeder is the level of ground plane of the main reflector. Surprisingly, that assumption proved to be working in case of small distance between the main reflector and slot array.

Besides of design of folded reflector antenna, design of simple reflector antenna having non-hyperbolic reflector was given. In this case, the method of phase center extraction proved to be applicable.

Acknowledgements

The authors thank M. Polívka from the Czech Technical University in Prague for performing simulations in IE3D. Research published in the paper has been financed by the grant no. 1929/2002 of the Czech Ministry of Education and by the research program MSM 262200011.

References

[1] POZAR, D. M., TARGONSKI, S. D., SYRIGOS, H. D. Design of Millimeter Wave Microstrip Reflectarrays. IEEE Transactions on Antennas and Propagation. 1997, vol. 45, no. 2, p. 287 - 295.

[2] MENZEL, W., PILZ, D. A 77-GHz FM/CW Radar Front-End with a Low-Profile Low Loss Printed Antenna. IEEE Trans. on Microwave Theory and Technique. 1999, vol.47, no. 12, p. 2237-2241.

[3] ENCINAR, J. A. Design of Two-Layer Printed Reflectarrays Using Patches of Variable Size. IEEE Transactions on Antennas and Propagation. 2001, vol. 49, no. 10, p. 1403 - 1410.

[4] FRANCHOIS, A., PICHOT, C. Microwave Imaging – Complex Permittivity Reconstruction with a Levenberg-Marquardt Method. IEEE Transact. on Antennas and Propagation. 1997, vol. 45, no. 2, p. 203 - 215.

[5] SCOTT, G. Spectral Domain Method in Electromagnetics. London: Artech House. 1989.

[6] GOŇA, S. A study of influence of dielectric cover on FSS properties. In Proceedings of the International Conference Radioelektronika 2002. Bratislava (Slovakia). 2002.

About authors...

Stanislav GOŇA was born in Slavičín in 1976. He received Ing (M.Sc.) degree in electrical engineering from Brno University of Technology (BUT) in 1999. He is currently postgraduate student at the Dept. of Radio Electronics at BUT. His research interests cover planar antennas, numerical modeling by method of moments and simulation of microwave structures in ANSYS.

Zbyněk RAIDA received Ing (M.Sc.) and Dr (Ph.D.) degrees from the Brno University of Technology (BUT) in 1991 and 94, respectively. From 1993 to 98, he was an assistant at the Dept. of Radio Electronics at BUT, and since 1999, he has been associated professor there. From 1996 to 1997, he spent 6 months at the Universite Catholique de Louvain. He is (co)author of more than 50 papers in journals and conference proceedings (modeling and optimization of EM structures).